


cambridge.org/mrf

Murari Shaw<sup>1</sup> , Niranjana Mandal<sup>2</sup> and Malay Gangopadhyay<sup>1</sup>

<sup>1</sup>Department of Electronics & Communication Engineering, Institute of Engineering & Management-Salt Lake, Kolkata-700091, West Bengal, India and <sup>2</sup>Controller of Examination, University of Engineering & Management, Newtown, West Bengal, India

## Research Paper

**Cite this article:** Shaw M, Mandal N, Gangopadhyay M (2021). A compact polarization reconfigurable stacked microstrip antenna for WiMAX application. *International Journal of Microwave and Wireless Technologies* **13**, 921–936. <https://doi.org/10.1017/S1759078720001567>

Received: 12 July 2020

Revised: 23 October 2020

Accepted: 27 October 2020

First published online: 27 November 2020

### Author for correspondence:

Murari Shaw, E-mail: [zmz\\_shaw@yahoo.co.in](mailto:zmz_shaw@yahoo.co.in)

### Abstract

In this paper, a stacked microstrip patch antenna with polarization reconfigurable property has been proposed for worldwide interoperability for microwave access (WiMAX) application. The proposed antenna has two substrate layers: upper and lower layers with two radiating patches connected with the coaxial probe. Without the upper layer the lower square-shaped substrate layer having regular hexagonal radiating patch with probe fed acts as a linear polarized antenna with impedance bandwidth for ( $S_{11} \leq -10$  dB) is 370 MHz 10.56% (3.32–3.69 GHz) cover WiMAX (3.4–3.69 GHz) application band. The hexagonal radiating patch is perturbed with an optimum rectangular slot to enhance the impedance bandwidth of the antenna. The lower substrate layer having hexagonal patch with the same probe position is stacked with the upper square-shaped substrate layer with same sized square patch and the upper patch soldered with the coaxial probe. The overall stacked antenna generates a circularly polarized band when the opposite corner of the top square radiating patch of the upper layer is truncated with optimum size. In order to generate another circularly polarized band and to improve the input impedance matching of the stacked antenna, the top radiating patch is perturbed with two slots and a slit. The stacked circularly polarized antenna generates impedance bandwidth of 12.75% (3.23–3.67 GHz) for ( $S_{11} \leq -10$  dB) with two circularly polarized bands (3.34–3.37 GHz) and (3.66–3.70 GHz) as per (axial ratio  $\leq 3$  dB) for WiMAX application. Therefore, the proposed antenna can be used as linearly polarized or dual band circularly polarized according to requirement.

## Introduction

Wireless communication technology is growing very fast and with this advancement requirement of the antenna with different properties also changes simultaneously, which cannot be fulfilled by the conventional antenna. Therefore, the reconfigurability of different properties of antenna as per the requirement with low profile becomes necessary for our current and future miniaturized communication devices. The communication devices are used in fixed places as well as in movable vehicles like cellular radio systems, wireless local area networks, mobile satellite systems etc. The fixed communication devices do not suffer from polarization mismatch loss, so a low profile linearly polarized antenna fulfills the requirement, but movable communication devices face multipath distortion, polarization mismatch loss along with transmitter and receiver orientation constraints. To overcome the above-mentioned problem circularly polarized antenna is required. Therefore, a low profile, compact, polarization reconfigurable antenna removes all the constraints and also very much fulfilling the requirement of advanced communication devices.

Many polarization reconfigurable antennas with different techniques and ideas have been published in the literature. Most of them are based on switching or tuning of electronic devices such as PIN diodes [1–3], varactor diodes [4] or radio frequency (RF) MEMS switches [5, 6] for opening or closing some sections of the antenna to change its polarization or resonant frequency [7–10]. Some of the reconfigurable antennas have used optical devices [11] or magnetic field tunable ferrites [12] or substrate with tunable properties like electric field tunable liquid crystals [13, 14]. Using actuators [15–20] mechanically reconfigurable antennas have been designed and some of the manually reconfigurable antennas [21–23] have also been designed in the past. Reconfiguration using electronic devices, optical devices, magnetically tunable ferrites and mechanical actuation is faster in speed but requires external circuits and power supply which made the designed antenna complex, costly, and larger in size, inconvenient for miniaturized communication technology. A manually reconfigurable antenna does not require external circuits or power supply may find applications where low cost, low profile, simple architecture, and quick fabrication is prioritized over switching speed.

This paper presents a manual polarization reconfigurable stacked microstrip patch antenna in which a linearly polarized antenna changes into dual-band circularly polarized when another substrate layer with the same sized square patch stacked on the linearly polarized

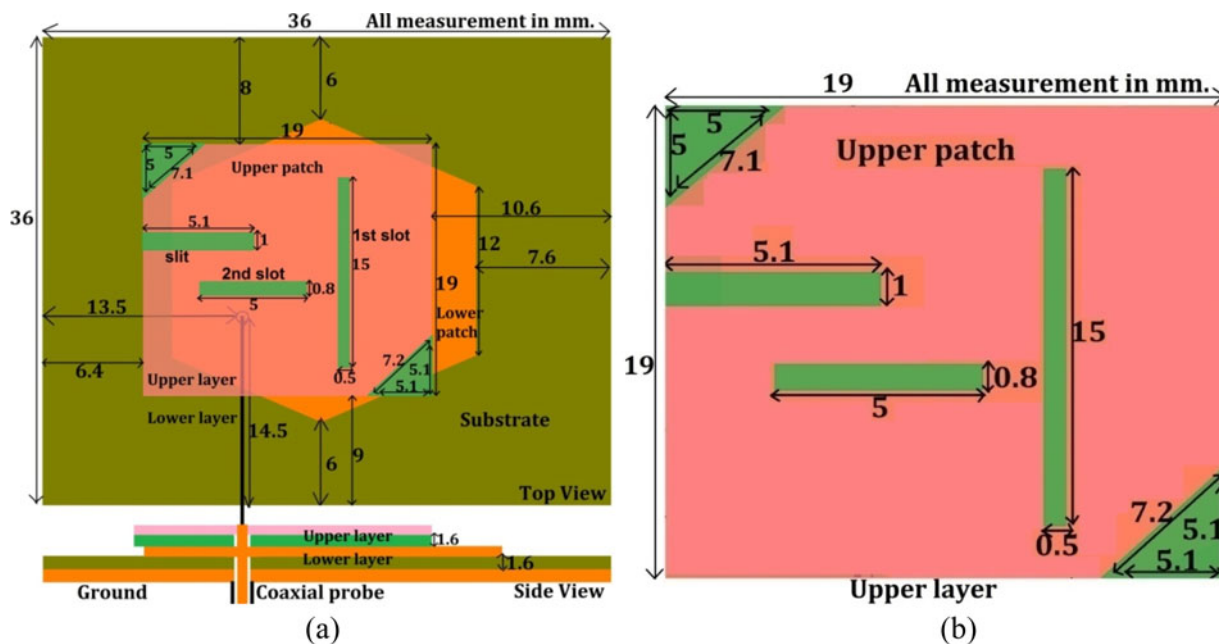


Fig. 1. Proposed antenna. (a) Final design and (b) upper layer.

lower layer antenna and the opposite corner of the top radiating patch is truncated with optimum size along with two slots and a slit. Without the upper layer, the lower square-shaped layer with regular hexagonal radiating patch acts as a linear polarized antenna having a broad impedance bandwidth of 10.56% and a low profile for worldwide interoperability for microwave access (WiMAX) (3.4–3.69 GHz) application band. With the addition of the upper layer, the final structure acts as dual-band circularly polarized antenna and generates impedance bandwidth 12.75% (3.23–3.67 GHz) for ( $S_{11} \leq -10$  dB) with two circularly polarized bands (3.34–3.37 GHz) and (3.66–3.70 GHz) for WiMAX application. So the complete structure comprises of both linearly and circularly polarized antennas with a low profile, compact, low fabrication cost, and reconfigurable property that can be used in our advanced communication devices without any space and polarization constraints and also fulfills the commercial requirement of the smaller antenna with multiple properties and low cost of fabrication.

### Antenna design

The proposed stacked microstrip patch antenna has two substrate layers, upper and lower layers with two radiating patches as shown in Figs 1(a) and 1(b). The lower square layer of  $36 \times 36 \times 1.6$  mm<sup>3</sup> dimension is comprised of a regular hexagonal patch with 12 mm side along with a rectangular perturbation of  $12 \times 0.6$  mm<sup>2</sup> size on the radiating patch. The upper square layer of  $19 \times 19 \times 1.6$  mm<sup>3</sup> dimension is comprised of pair of opposite corner truncated square patch with two slots of  $15 \times 0.5$  mm<sup>2</sup> and  $5 \times 0.8$  mm<sup>2</sup> dimension and a slit of  $5.1 \times 1$  mm<sup>2</sup> size on the radiating patch. The length of two opposite truncated corners of the top radiating patch is 7.1 and 7.2 mm. Lower radiating patch, top radiating patch, and ground plane have been made using thin copper sheet and FR4 material of 1.6 mm height has been used for both lower and upper layers as a dielectric substrate with  $\epsilon_r = 4.4$  and  $\tan \delta = 0.02$ . A probe of 50  $\Omega$  impedance with an

SubMiniature version A (SMA) connector situated 13.5 mm from the left edge and 14.5 mm from the bottom edge of the substrate has been used to excite the proposed antenna.

### Antenna design procedure with parametric study

During the designing process of the proposed antenna supposed to operate in the WiMAX (3.4–3.69 GHz) application band, many combinations of side lengths of the regular hexagonal radiating patch along with mathematical equations (1) and (2) [24] given below have been used to compute the resonant frequency. After parametric calculation with different side lengths, at 12 mm side lengths the primary resonant frequency is 3.84 GHz near to the desired result. Regular hexagonal patch antenna and circular patch antenna are very closely related to each other. Consequently, the resonant frequency of a circular patch antenna (1) along with (2) has been used to calculate the primary resonant frequency of the hexagonal patch antenna

$$f_r = \frac{X_{mn}}{2\pi a_e \sqrt{\epsilon_r}} c, \tag{1}$$

where  $f_r$  is the resonant frequency of the circular patch antenna;  $X_{mn} = 1.8411$  for the dominant mode  $TM_{11}$ ;  $c$  is the velocity of light in free space;  $\epsilon_r$  is the relative permittivity of the substrate and  $a_e$  is the effective radius of the circular patch

$$\pi a_e^2 = \frac{3\sqrt{3}}{2} s^2, \tag{2}$$

where  $s$  is the side length of the regular hexagonal patch.

After calculating 3.84 GHz as the resonant frequency of the conventional regular hexagonal patch antenna with 12 mm sides, it has been designed and analyzed using simulation software (HFSS ver.13) for finding the impedance bandwidth of the primary resonant frequency. With the co-axial probe position

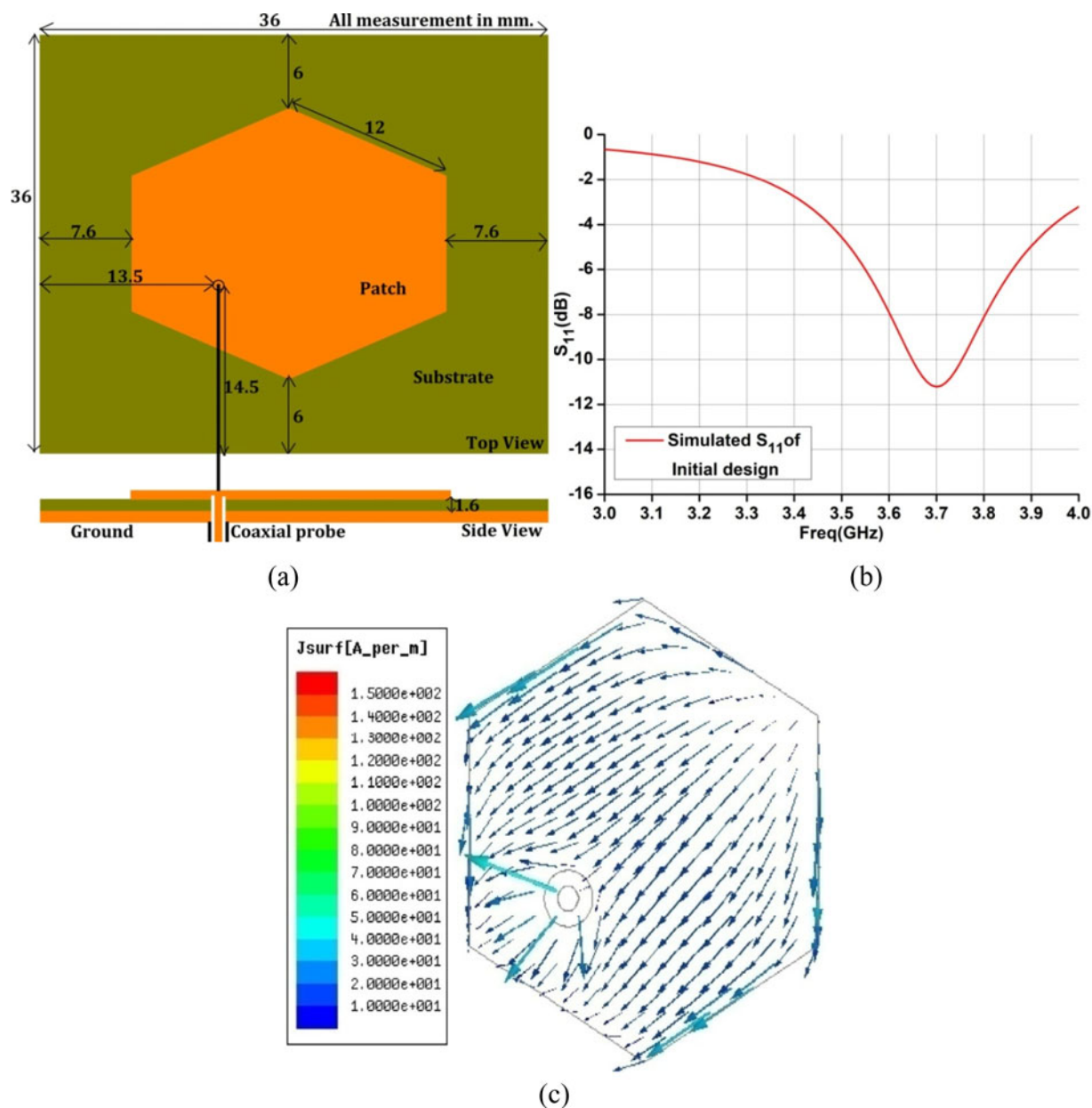


**Fig. 2.** (a) Initial design of the proposed antenna with probe position 13.5 mm from the left edge and 14.5 mm from the bottom edge of the substrate. (b)  $S_{11}$  of the antenna at the above-mentioned probe position. (c) Current distribution (simulated) on the radiating surface of the antenna at 3.7 GHz frequency.

(13.5 mm from the left edge and 14.5 mm from the bottom edge of the substrate) the impedance bandwidth for ( $S_{11} \leq -10$  dB) is 100 MHz (3.65–3.75 GHz) as shown in Figs 2(a) and 2(b). Current distribution on the radiating surface of the antenna at 3.7 GHz frequency is also shown in Fig. 2(c).

The above conventional hexagonal patch antenna is not suitable for any application; therefore, it has been slotted so that it can be used for desired application band.

### Effect of slot

The addition of slot on the radiating patch generates higher-order mode because the loading of the patch with the slot causes inclusion of capacitive reactance with it forms a parallel Inductive and capacitive (LC) resonance with stray patch inductances leading to

an additional resonant band which when overlaps with the fundamental mode, enhances the overall bandwidth of the antenna and thus the surface current path length increases that causes a shift of resonant frequency towards the lower frequency range [25–29]. It also decreases the input impedance and causes improvement in impedance matching.

Based on this concept, in order to enhance the bandwidth and lowering of the primary resonant frequency of the conventional antenna so that it can fully cover the desired application band, the patch has been loaded with a rectangular slot. A parametric simulation has been done with 0.6 mm width and various lengths of the slot using high-frequency structure simulator and  $S_{11}$  and input impedance has been observed. Changes of resonant frequency, bandwidth, and input impedance with different slot lengths are shown in Figs 3(a) and 3(b). With  $12 \times 0.6$  mm<sup>2</sup> slot

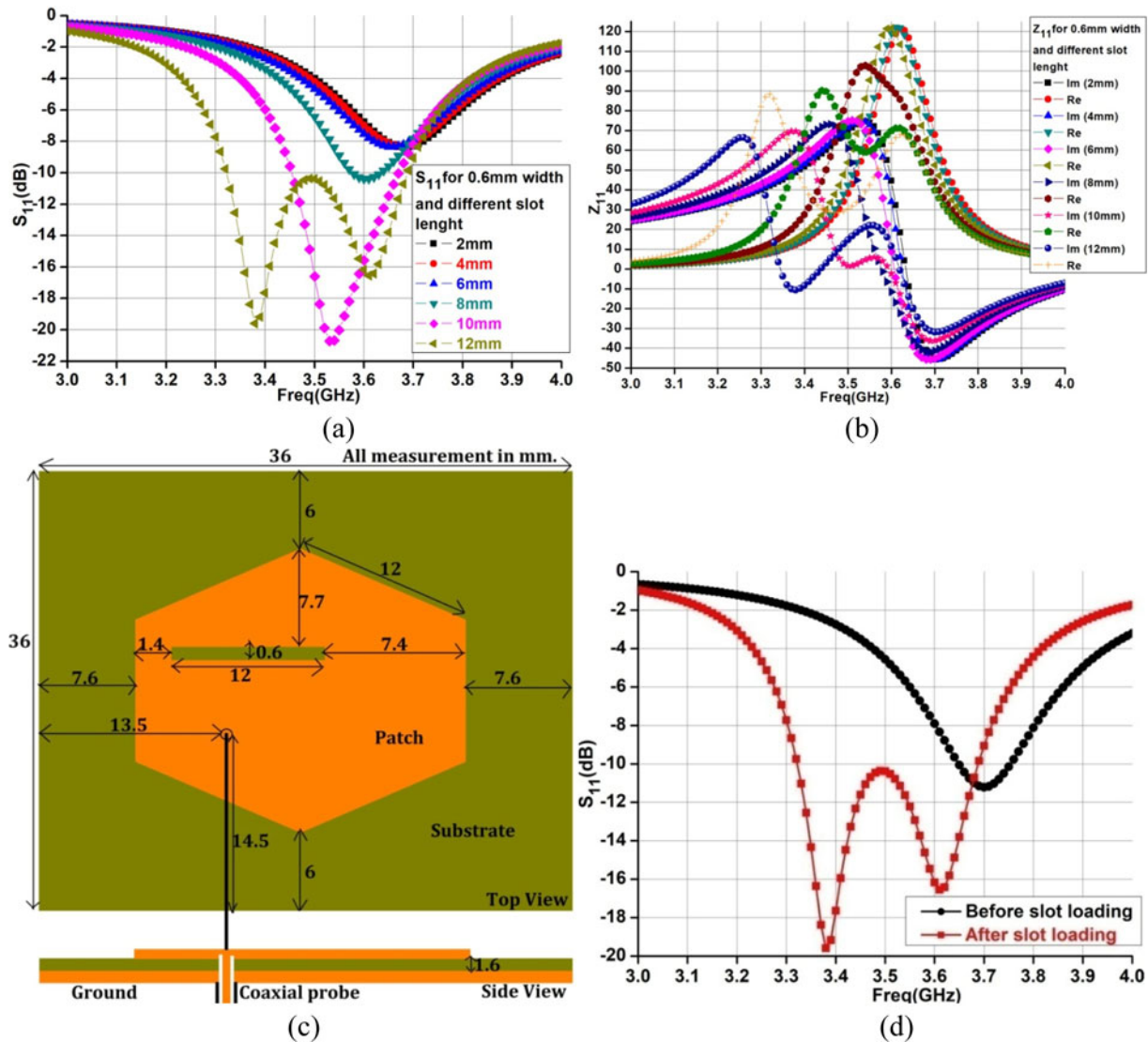


**Fig. 3.** (a) Changes of the resonant frequency and bandwidth with the change in slot length having constant 0.6 mm width. (b) Changes of the input impedance with the change in slot length having constant 0.6 mm width. (c) Final design of lower layer antenna with the optimized rectangular slot. (d)  $S_{11}$  before and after the addition of a rectangular slot. (e)  $Z_{11}$  before and after the addition of a rectangular slot. (f) & (g) Current distribution (simulated) on the radiating surface of the antenna at 3.38 and 3.61 GHz frequencies.

dimension and a distance of 7.7 mm from the top vertex and 1.4 mm from the left side of the hexagonal patch as shown in Figs 3(c)–3(e) the antenna operating band turns out to be (3.32–3.69 GHz) which exactly covers the WiMAX (3.4–3.69 GHz) application band. Also, primary resonant frequency shifted from 3.7 to 3.38 GHz yielding about 8.7% antenna miniaturization. Therefore, this linearly polarized rectangular slotted hexagonal patch antenna with a gain of 2.2 dB at 3.69 GHz can be used for the above-mentioned application band. Current distribution on the radiating surface of the antenna at 3.38 and 3.61 GHz frequencies are also shown in Figs 3(f) and 3(g).

Measured results of the fabricated antenna and software simulated results of the linearly polarized lower layer antenna have been given in Table 1.

Different measured and simulated parameters of the linearly polarized lower layer antenna are shown in Figs 4–8.

Measured and software simulated input impedance of the antenna as shown in Fig. 7.

The gain and  $S_{11}$  curves seem contradictory, as the gain is still going up at the higher end of the spectrum. The gain plot shown in Fig. 8(a) of the paper is the total gain of the antenna excluding the mismatch effects. On the other hand, the realized gain as shown in Fig. 8(c) contains the mismatch losses. It can be seen from Fig. 8(c) that the realized gain has appreciable magnitude only inside the operating band (3.32–3.69 GHz) of the structure. Outside the operating band when the return loss ( $S_{11}$ ) increases, the realized gain reduces, as expected.

An explanation for the monotonically increasing radiation efficiency is similar to the gain case above. Radiation efficiency is defined as the ratio of power radiated to the power accepted by the antenna. It does not include the mismatch losses. On the other hand, the antenna efficiency includes the mismatch losses at the antenna input terminal and is consequently defined as the ratio of the power radiated to the total power incident on the antenna. As can be seen from Fig. 8(d), the antenna efficiency for the proposed antenna follows the intuitively understandable



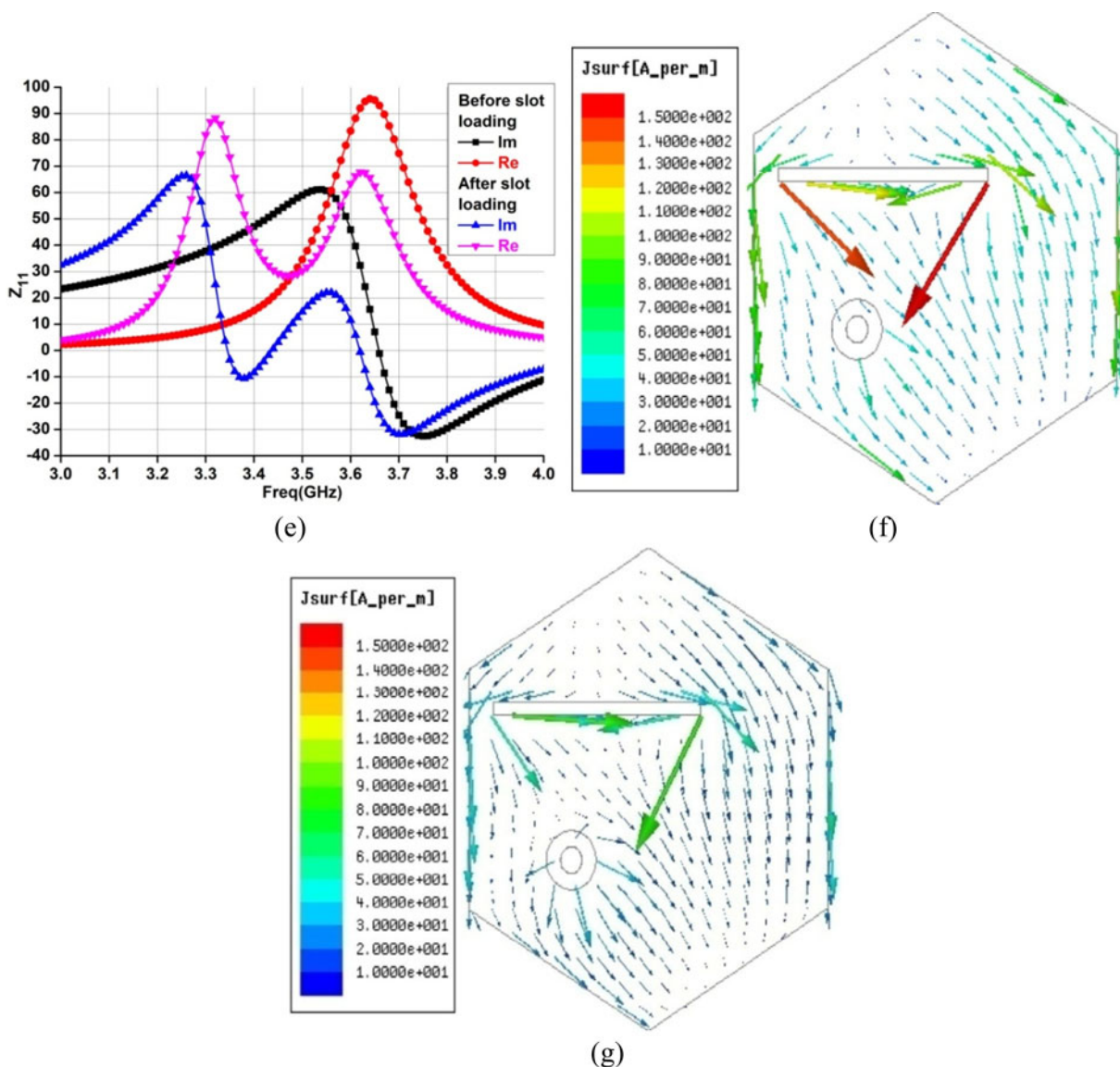


Fig. 3. Continued.

Table 1. Software simulated and fabricated measured result of the linearly polarized antenna.

Parameters	Simulated	Measured
Impedance bandwidth ( $S_{11} \leq -10$ dB)	(3.32–3.69 GHz) 370 MHz	(3.34–3.7 GHz) 360 MHz
Impedance bandwidth (%)	10.56%	10.23%
Peak gain (dB)	2.2 at 3.69 GHz	2 at 3.69 GHz
Efficiency (%)	86 at 3.5 GHz	85 at 3.5 GHz
Application	<b>WiMAX (3.4–3.69 GHz)</b>	

behavior of almost constant in the operating band (3.32–3.69 GHz) and reducing outside the operating band.

Radiation pattern shows the radiation characteristics of the antenna as a function of space coordinate. The performance of

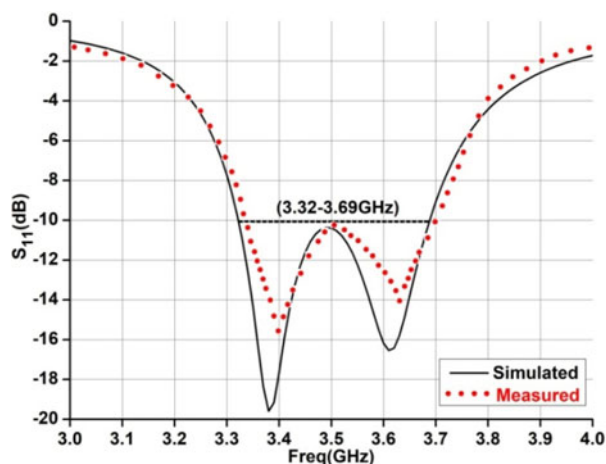


Fig. 4.  $S_{11}$  (measured and simulated) of the lower layer antenna.

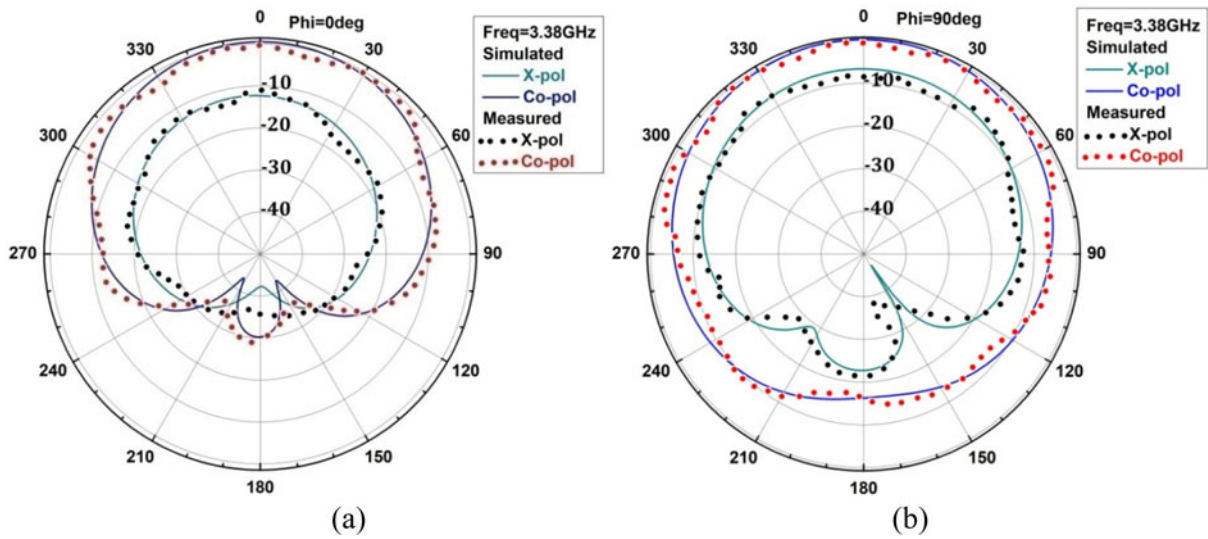


Fig. 5. Radiation pattern (a) *E*-plane and (b) *H*-plane at 3.38 GHz frequency.

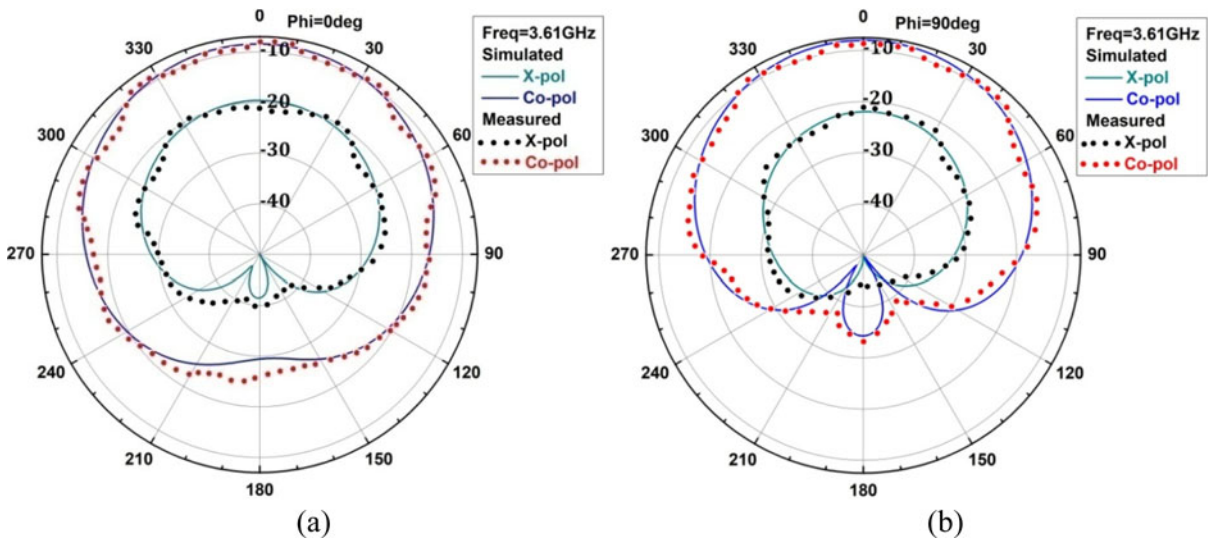


Fig. 6. Radiation pattern (a) *E*-plane and (b) *H*-plane at 3.61 GHz frequency.

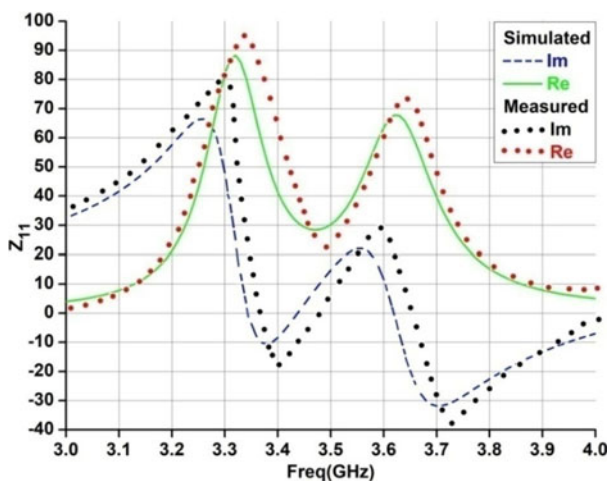


Fig. 7. Measured and software simulated input impedance of the antenna.

linearly polarized antennas is often described in terms of *E* and *H*-planes. The *E* and *H*-planes are defined as the radiating planes containing the electric field vector (co-pol and x-pol) and the magnetic field vector (co-pol and x-pol). Figures 5 and 6 show the software simulated and fabricated measured co-pol and x-pol in two-dimensional *E* and *H*-planes at 3.38 and 3.61 GHz frequencies with  $\Phi = 0^\circ$  and  $90^\circ$  and theta ( $\theta$ ) between  $0^\circ$  and  $360^\circ$ . It can be seen from Figs 5 and 6 that the proposed antenna has broadside radiation pattern with co-pol and x-pol 12.5 and 11.3 dB at 3.38 and 3.61 GHz frequencies which is in the acceptable range.

### Equivalent circuit modal

To provide an enhanced insight and physical analysis into the designed antenna, an equivalent circuit model representing the functioning of the antenna has been shown in Figs 9 and 10. The circuit model has been developed by fitting the simulation

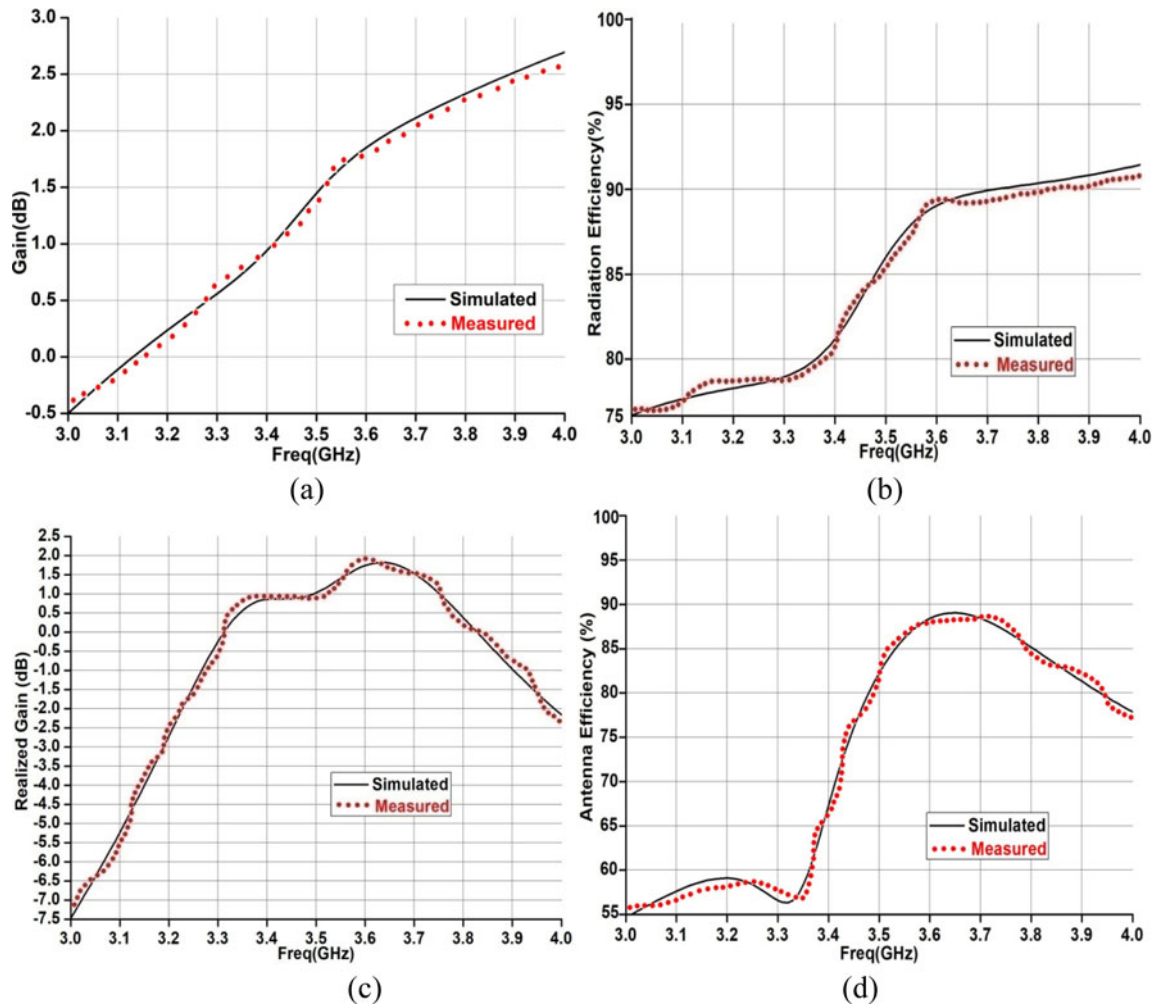


Fig. 8. (a) Measured and software simulated gain of the antenna. (b) Measured and software simulated radiation efficiency of the antenna. (c) Measured and software simulated realized gain of the antenna. (d) Measured and software simulated antenna efficiency.

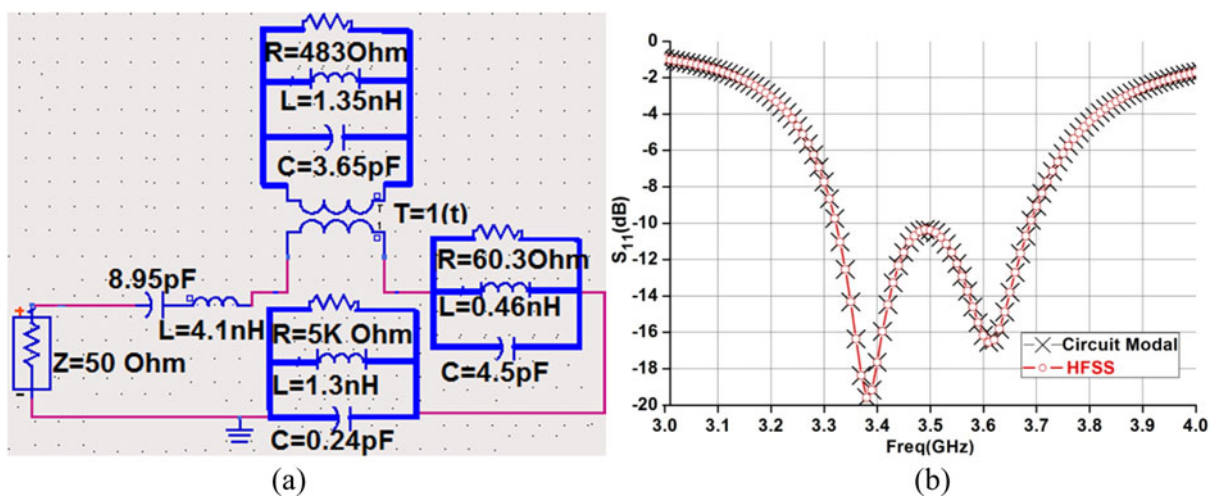


Fig. 9. (a) Equivalent circuit model of lower layer antenna. (b) Comparison of  $S_{11}$  of equivalent circuit model with  $S_{11}$  of HFSS.

S-parameters into the prototype circuits and using ADS Software. The equivalent circuit is basically a higher-order multi-pole circuit with multiple inductors and capacitors. The circuit is made

under the assumption that a higher-order circuit model is required to model the frequency sensitive and high Q nature of the S-parameter of the original circuit. Consequently, the



## A) Equivalent circuit modal

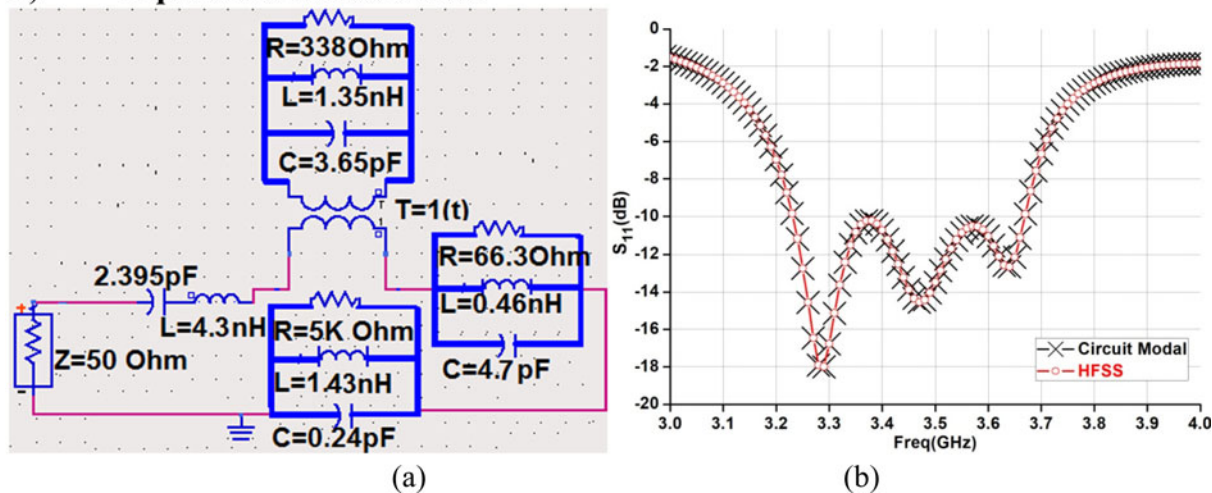


Fig. 10. (a) Equivalent circuit model of final proposed antenna. (b) Comparison of  $S_{11}$  of equivalent circuit model with  $S_{11}$  of HFSS.

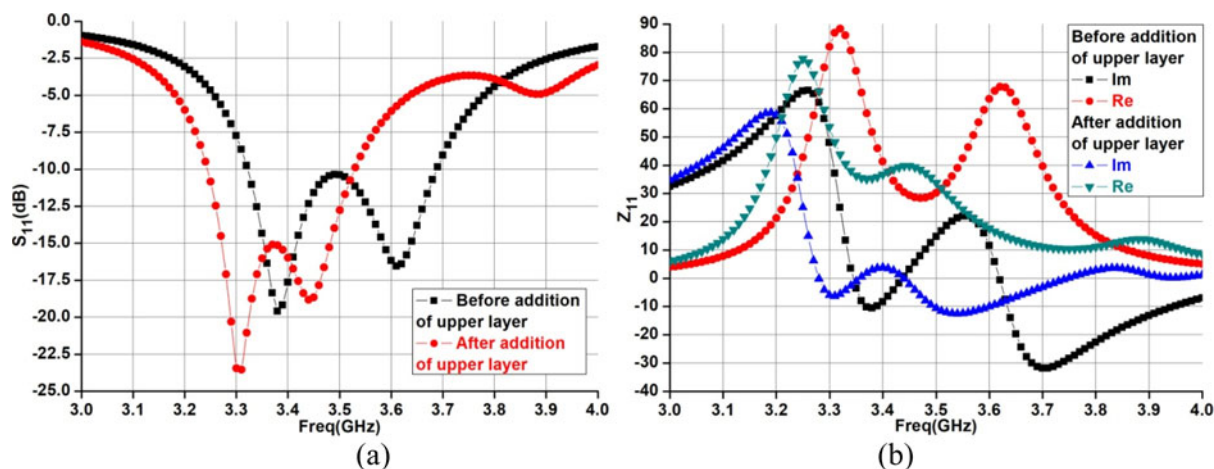


Fig. 11. (a)  $S_{11}$  of the designed antenna before and after the addition of the upper layer. (b) Input impedance before and after the addition of the upper layer. (c) Changes of axial ratio with different corner truncation area. (d, e, f, and g) Current distribution (simulated) on the surface at 3.35 GHz frequency for different time instants. (h) Design of the antenna after the addition of the upper layer and corner truncation. (i)  $S_{11}$  after the addition of the upper layer and corner truncation.

prototype circuit is not a physical model but rather an empirical one imitating the original circuit terminal behavior.

The linearly polarized patch antenna suffering from multipath distortion and polarization mismatch loss requires the circularly polarized antenna to overcome these problems. Therefore, in order to convert the above-designed antenna into the circularly polarized antenna and also to further improve the performance, another square-shaped substrate layer along with the same shape and size radiating patch has been placed on the lower substrate layer and the upper radiating patch soldered with the coaxial probe. After that, the opposite corner of the top radiating patch is truncated and the two slots and a slit are also introduced.

#### Effect of addition of upper substrate layer and corner truncation

The addition of upper layer decreases the input impedance of the overall structure causing improvement in impedance matching

and lengthening of the surface current path that causes a shift of resonant frequency towards the lower frequency range, which can be seen in Figs 11(a) and 11(b). The size of the upper substrate along with patch has been optimized by varying the size of it and observing the corresponding results of  $S_{11}$  and input impedance. The optimum size has been found to be  $19 \times 19 \text{ mm}^2$  and increasing it beyond this gives undesired results.

Next, in order to change the polarization of the overall structure from linear to circular, the opposite corner of the top square radiating patch has been truncated. The opposite corner truncation generates two near degenerate modes with  $90^\circ$  out of phase [30–32] and also alters the surface current distribution leading to the generation of the circularly polarized wave. The truncation amount of the corner controls the relative phase of the degenerate modes. Based on this concept, a parametric simulation on the corner truncation amount has been done using the simulator software and the axial ratio has been observed. Changes of the axial ratio with the amount of corner truncation and the current



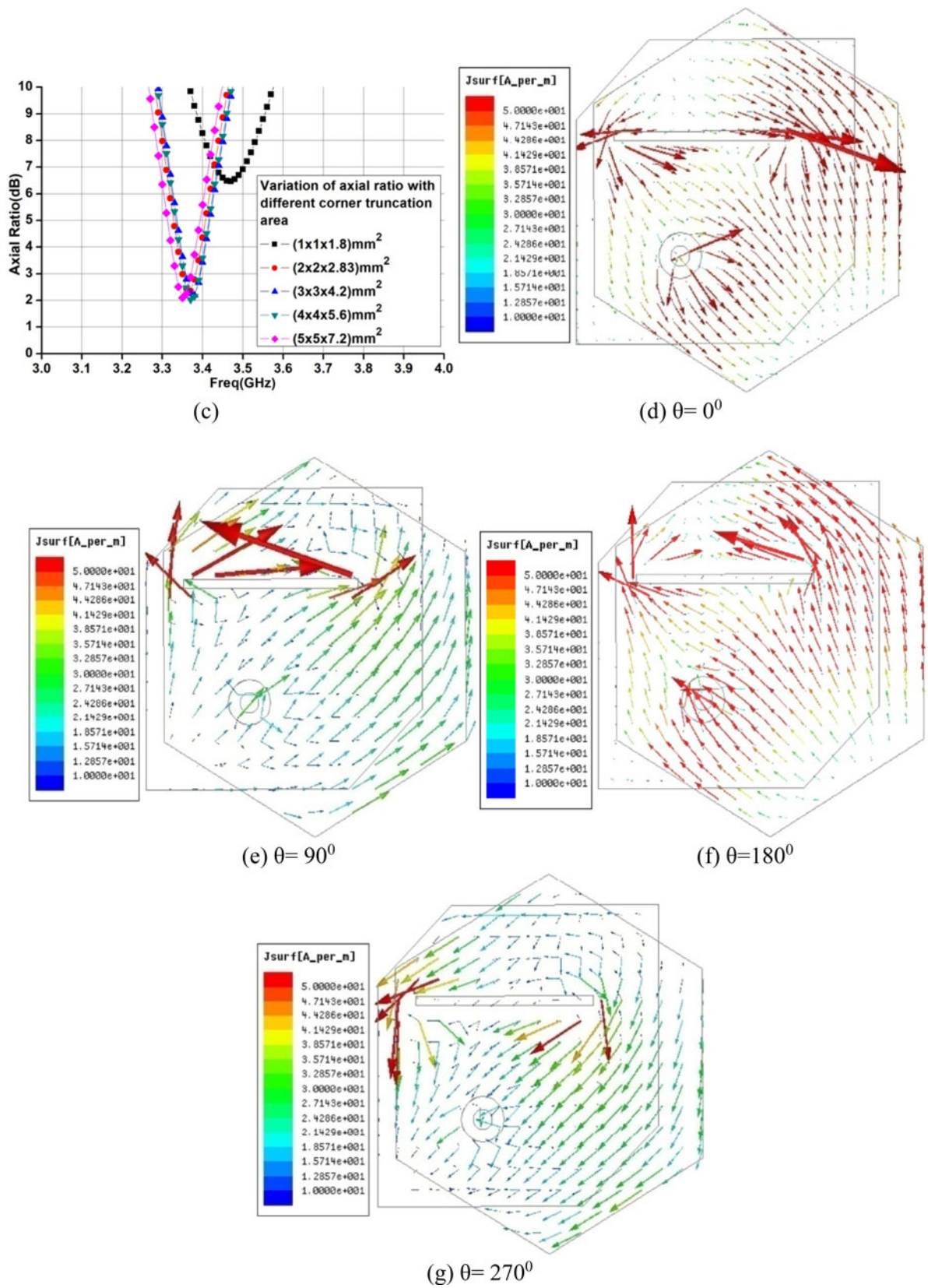


Fig. 11. Continued.

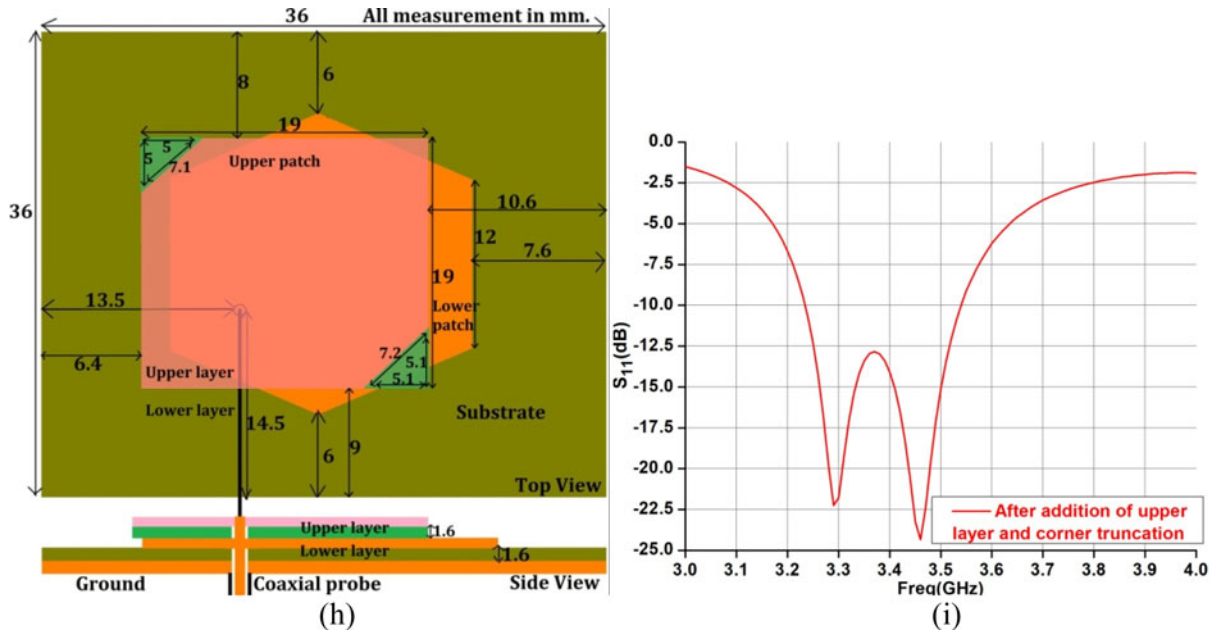


Fig. 11. Continued.

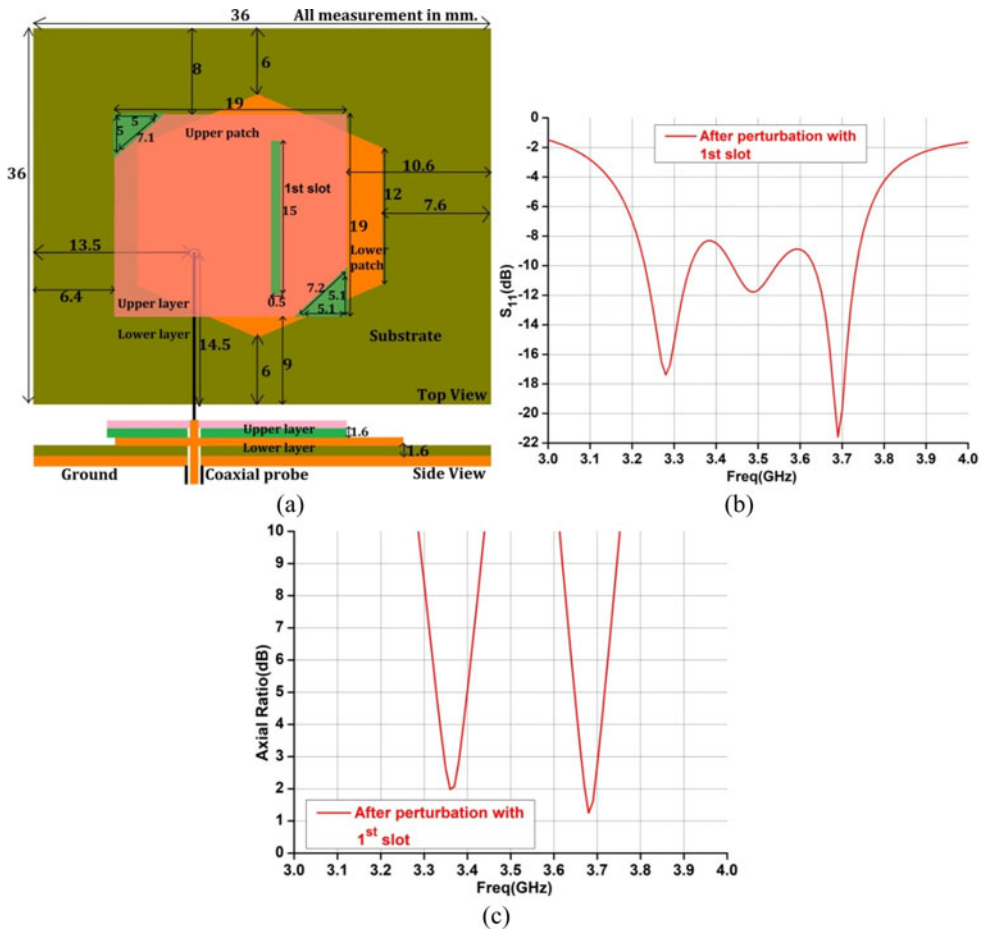


Fig. 12. (a) Design of the stacked antenna after first slot on the top radiating patch. (b)  $S_{11}$  of the stacked antenna after first slot on the top radiating patch. (c) The axial ratio of the stacked antenna after first slot on the top radiating patch.

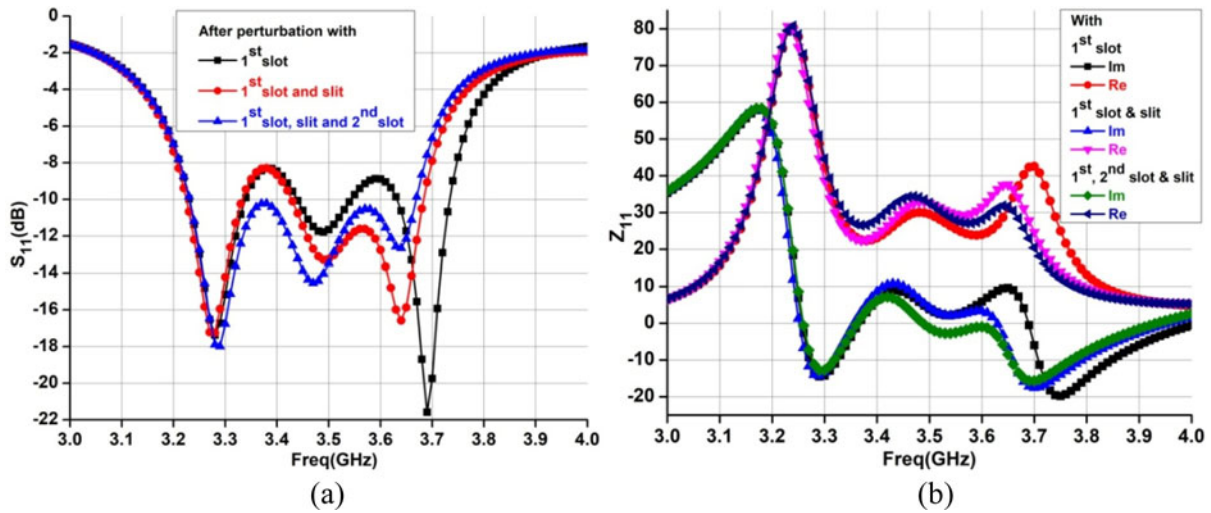


Fig. 13. (a)  $S_{11}$  and (b) Input impedance of the antenna after perturbation with first slot, second slot and slit on the top patch of the upper layer.

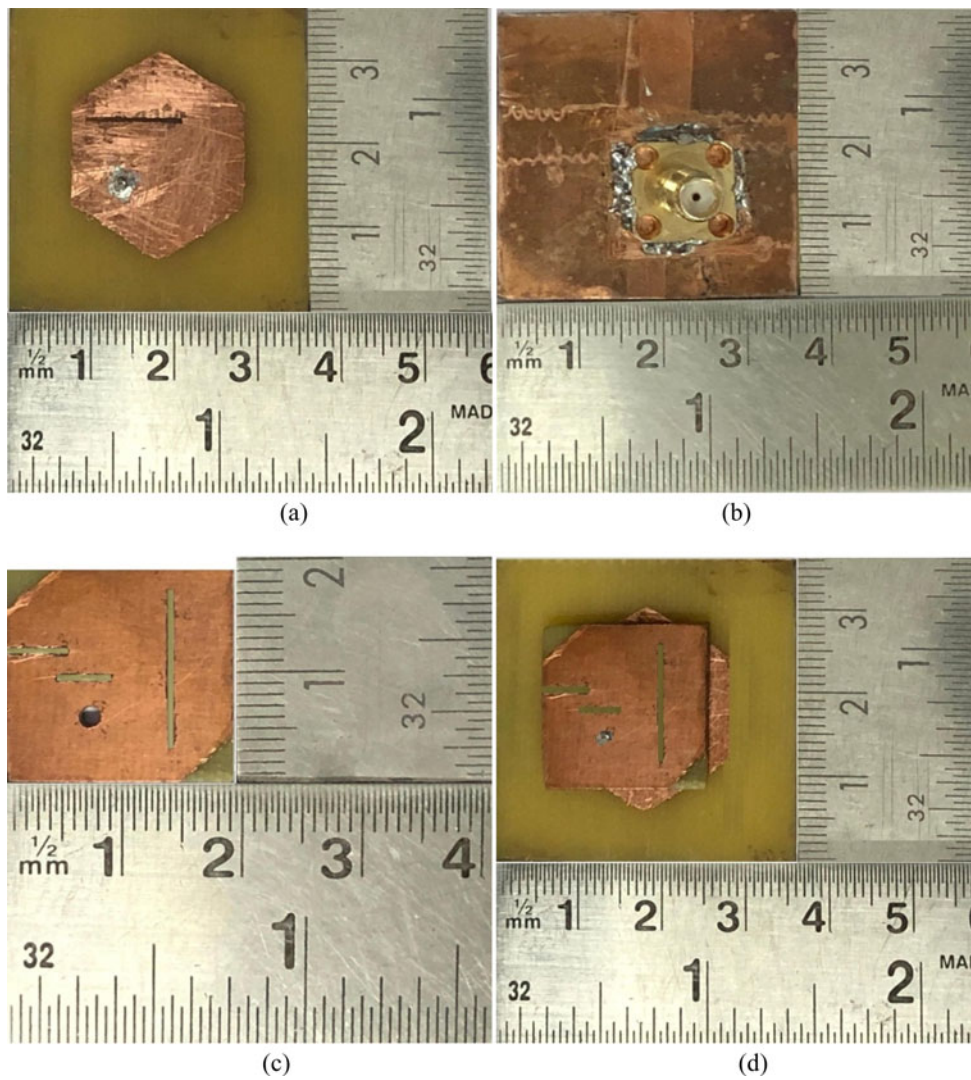
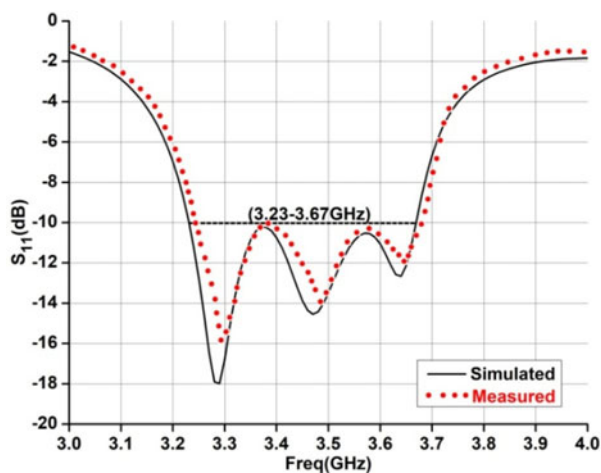


Fig. 14. Photograph of fabricated prototype antenna. (a) Top view of the lower layer. (b) Bottom view of lower layer. (c) Top view of upper layer. (d) Top view of the complete stacked antenna.



**Table 2.** Simulated and measured result of the circularly polarized antenna.

Parameters	Simulated	Measured
Impedance bandwidth ( $S_{11} \leq -10$ dB)	(3.23–3.67 GHz) 440 MHz	(3.25–3.68 GHz) 430 MHz
Impedance bandwidth (%)	12.75%	12.4%
Circularly polarized bandwidth (Axial ratio $\leq 3$ dB)	(3.34–3.38 GHz) 40 MHz & (3.64–3.68 GHz) 40 MHz	(3.36–3.39 GHz) 30 MHz & (3.66–3.69 GHz) 30 MHz
Circularly polarized bandwidth (%)	1.2 & 1.1	0.9 & 0.82
Peak gain (dB)	1.84 at 3.54 GHz	1.81 at 3.54 GHz
Efficiency (%)	82% for CP (first band) 86.2% for CP (second band)	80.5% for CP (first band) 84.2% for CP (second band)
Application	<b>1. WiMAX (3.3–3.4 GHz)</b> <b>2. WiMAX (3.4–3.69 GHz)</b>	

**Fig. 15.** Software simulated and fabricated measured  $S_{11}$  of the antenna.

distribution on the surface at 3.35 GHz frequency for different time instants are shown in Figs 11(c)–11(g).

In this way, a linearly polarized antenna becomes circularly polarized with circularly polarized bandwidth 0.9% (3.34–3.37 GHz) for (axial ratio  $\leq 3$  dB) and impedance bandwidth for ( $S_{11} \leq -10$  dB) is 300 MHz 8.85% (3.24–3.54 GHz) as shown in Figs 11(h) and 11(i).

### Effect of first slot on the top radiating patch

In order to enhance the bandwidth of the above circularly polarized antenna so that it can cover more application bands, the top patch has been loaded with a rectangular slot. The size and position of the slot have been optimized by varying the size and position on the radiating patch and observing the corresponding results. With  $15 \times 0.5$  mm<sup>2</sup> slot dimension and position as shown in Fig. 1, the stacked antenna operating band turns out to be (3.23–3.74 GHz). Therefore, impedance bandwidth for ( $S_{11} \leq -10$  dB) becomes 510 MHz 14.63% and enhanced by 5.8% with the generation of another circularly polarized band (3.66–3.70 GHz) for (axial ratio  $\leq 3$  dB) as shown in Figs 12(a)–12(c) due to reason mentioned in (section ‘Effect of a slot’).

### Effect of second slot and slit on the top radiating patch

It can be observed from Fig. 12(b), some portion of (3.23–3.74 GHz) frequency band has a return loss of more than ( $-10$  dB) due to high input impedance leading to poor impedance matching.

Perturbation of the top radiating patch with optimized slit and second slot as shown in Fig. 1 decreases the input impedance between the said bandwidth. Therefore, the input impedance shifted near  $50 \Omega$  value, as shown in Figs 13(a) and 13(b) and the satisfactory impedance matching and axial ratio ( $S_{11}$ ) are obtained in the bandwidth.

These are the above-mentioned procedures which have been used to design the final structure of the antenna. A prototype of the final structure has been fabricated as shown in Figs 14(a)–14(d) and different parameters of the antenna have been measured using VNA bench top (Model No.E5071B) and anechoic chamber.

## Results

The software simulated and fabricated measured result of the final circularly polarized antenna has been given in Table 2.

A very good resemblance has been seen between the software simulated and fabricated measured results of the return loss, axial ratio, input impedance, radiation pattern, and gain of the prototype antenna as shown in Figs 15–19. However, a very small shift can be observed in the measured results because of improper connector soldering, absence of ideal measuring environment [33], and inhomogeneous dielectric constant of the substrate [34], which is not considered at the time of the simulation. The performance of the circularly polarized antennas is often described in terms of  $E$ -plane ( $X$ - $Z$ ) and  $H$ -plane ( $Y$ - $Z$ ). The  $E$ - and  $H$ -planes are defined as the radiating planes containing the electric field vector (RHCP and LHCP) and the magnetic field vector (RHCP and LHCP). Figures 16(a)–16(d) show the simulated and measured RHCP and LHCP in two-dimensional  $E$  and  $H$ -planes at 3.36 and 3.6 GHz frequencies with  $\Phi = 0^\circ$  and  $90^\circ$  and theta ( $\theta$ ) between  $0^\circ$  and  $360^\circ$ . It can be seen from Figs 16(a)–16(d) that the proposed antenna has good difference between RHCP and LHCP in both  $E$ -plane and  $H$ -plane.

The gain of the proposed antenna is little low because the substrate used in the antenna is FR4 which is the lossy substrate. Therefore, it is one of the reasons for low gain of the antenna.

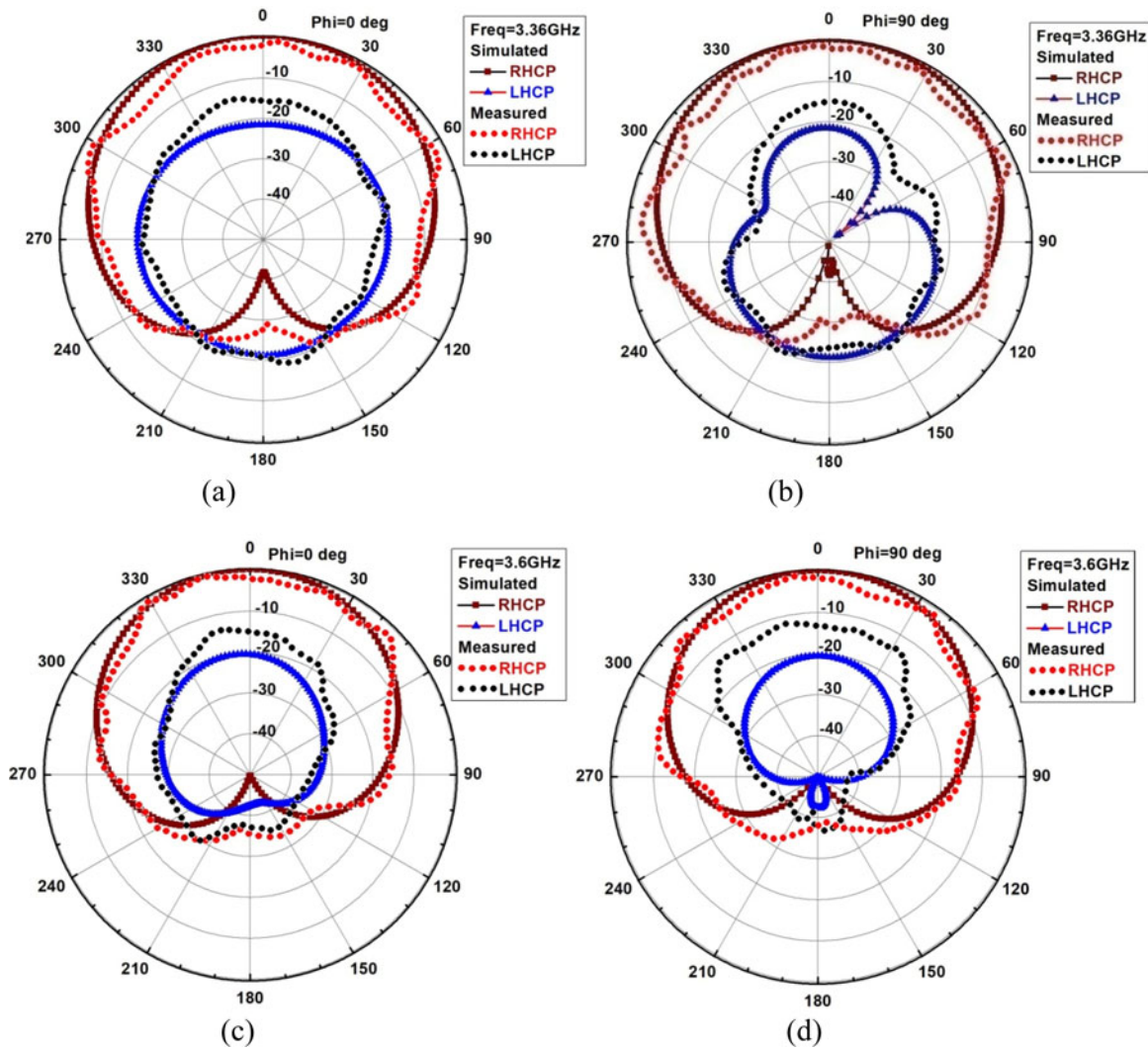


Fig. 16. (a and b) Radiation pattern (Normalized) X-Z and Y-Z planes at 3.36 GHz. (c and d) Radiation pattern (Normalized) X-Z and Y-Z planes at 3.6 GHz.

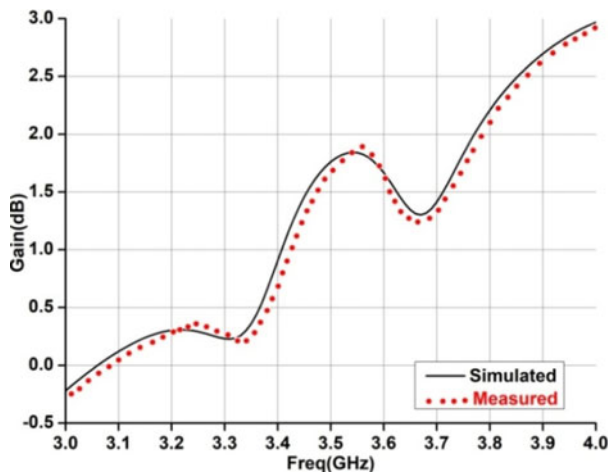


Fig. 17. Measured and simulated gain of the antenna.

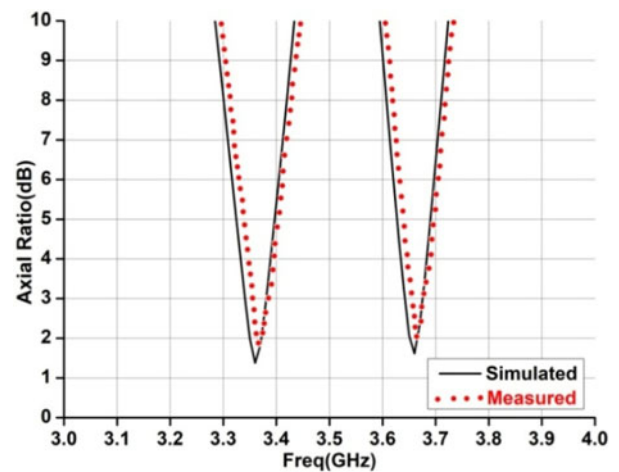


Fig. 18. Axial ratio of the antenna.

Another reason is that, a constant (input excitation) amount of power is distributed to all operating bands of the antenna. Achievement of a circularly polarized radiation necessitated the

excitation of two closely spaced orthogonal modes in the designed antenna. Consequently, input power is distributed between these two modes and subsequent interaction between the radiated

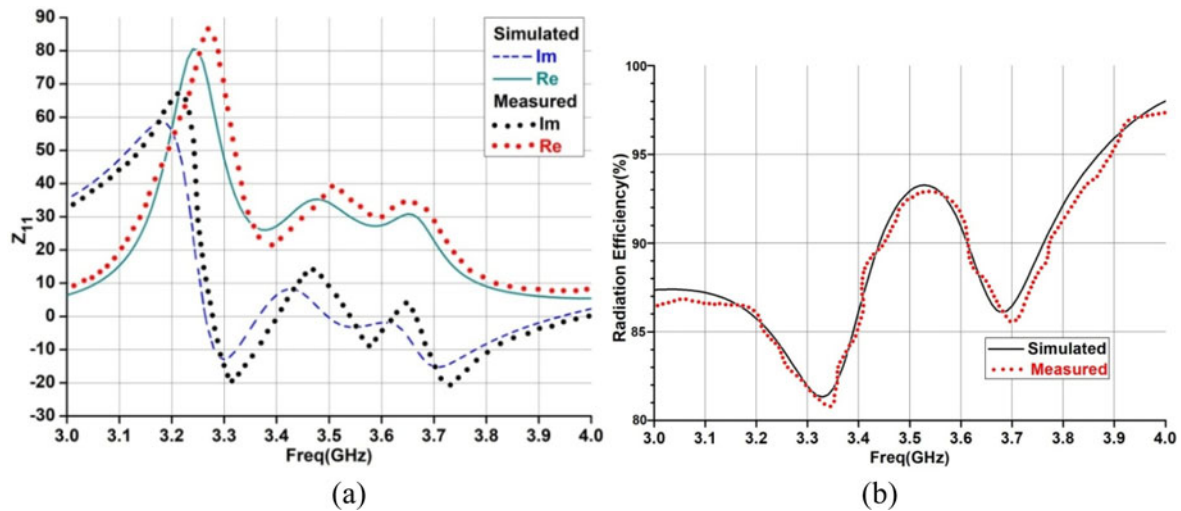


Fig. 19. (a) Measured and simulated input impedance of the antenna. (b) Measured and simulated radiation efficiency of the antenna.

Table 3. Comparison of proposed antenna performance with existing cases in literature.

Ref no.	Antenna size ( $\lambda_0 \times \lambda_0 \times \lambda_0$ ) At	Linear polarization		Circular polarization			Efficiency
		Impedance BW ( $S_{11} \leq -10$ dB)	Gain	Impedance BW ( $S_{11} \leq -10$ dB)	ARBW (AR $\leq 3$ dB)	Gain	
[35]	1.05 × 0.93 × 0.03 At 9.75 GHz	175 MHz, 1.8% 9.65–9.83 GHz	6.45 dBi	530 MHz, 5.32% 9.61–10.14 GHz	140 MHz, 1.4% 9.82–9.96 GHz	6.33 dBic	–
[36]	1.05 × 0.94 × 0.02 At 3.08 GHz	40 MHz, 1.3% 3.06–3.10 GHz	7.74 dBi	80 MHz, 2.58% 3.06–3.14 GHz	10 MHz, 0.3% 3.12–3.13 GHz	8 dBi	–
[37]	0.39 × 0.39 × 0.013 At 2.35 GHz	100 MHz, 4.2% 2.31–2.41 GHz	6.2 dBi	100 MHz, 4.25% 2.31–2.41 GHz	140 MHz, 5.95% 2.3–2.44 GHz	5.82 dBic	71% for LP 66% for CP
[38]	0.57 × 0.28 × 0.013 At 5.2 GHz	103 MHz, 1.9% 5.16–5.26 GHz	7 dBi	75 MHz, 1.5% 5.18–5.26 GHz	80 MHz, 1.6% 5.16–5.24 GHz	7.3 dBic	–
[39]	1.34 × 1.34 × 0.04 At 8.05 GHz	190 MHz, 2.4% 7.98–8.17 GHz	5.95 dBi	500 MHz, 6.1% 7.95–8.45 GHz	260 MHz, 2.83% 8.12–8.38 GHz	6.16 dBic	71.6% for LP 59.9% for CP
[40]	2.06 × 2.06 × 0.054 At 10.3 GHz	680 MHz, 6.6% 10.3 GHz	7.8 dBi	680 MHz, 6.6% 10.3 GHz	265 MHz, 2.57% 10.05–10.3 GHz	7.65 dBic	–
[41]	0.64 × 0.64 × 0.06 At 2.4 GHz	30 MHz, –% –	5.83 dB	60 MHz, –% –	20 MHz, –% –	6.4 dB	–
[42]	0.79 × 0.79 × 0.06 At 5.9 GHz	360 MHz, 6.1% 5.72–6.08 GHz	6.25–7.3 dBi	700 MHz, 13.5% 5.6–6.3 GHz	160 MHz, 2.8% 5.7–5.86 GHz	6.3–7.5 dBic	73% for LP 82% for CP
This work	0.4 × 0.4 × 0.04 At 3.3 GHz	370 MHz, 10.56% 3.32–3.69 GHz	2.2 dB	440 MHz, 12.75% 3.23–3.67 GHz	40 MHz, 1.2% 3.34–3.38 GHz & 40 MHz, 1.1% 3.64–3.68 GHz	1.84 dB	86% for LP 82% for CP (first band) 86.2% for CP (second band)

Where  $\lambda_0$  is the free space wavelength.

far-fields from these two modes lead to an eventual reduction in the overall gain of the antenna.

### Equivalent circuit modal

A performance comparison of the proposed work with previously reported work, those available in the literature is presented in Table 3, shows the merit of the proposed antenna.

### Conclusion

A stacked microstrip patch antenna having two square substrate layers and two radiating patches with polarization reconfigurable property has been designed for the WiMAX application. Lower square substrate layer having regular hexagonal radiating patch acts as a linear polarized antenna with impedance bandwidth of 10.56% (3.32–3.69 GHz) cover WiMAX (3.4–3.69 GHz) application band. Also, the theoretical calculation has been done with various



combinations of side lengths of the regular hexagonal patch and mathematical equation to find the desired resonant frequency of the conventional hexagonal microstrip patch antenna. The hexagonal radiating patch perturbed with an optimum rectangular slot to enhance the impedance bandwidth. After the lower layer stacked with the upper layer and opposite corner of the top radiating patch truncated, then the antenna becomes circularly polarized. The top radiating patch also perturbed with two slots and a slit in order to generate another resonant band along with improvement in impedance matching and  $S_{11}$ . Therefore, the stacked antenna generates two circularly polarized resonant bands with impedance bandwidth of 12.75% (3.23–3.67 GHz) for WiMAX application. Equivalent circuit model for both linearly polarized and circularly polarized antenna also given for better insight of the proposed antenna. Therefore, the complete structure has both linearly and circularly polarized antennas with a low profile, compact, low cost, and reconfigurable property suitable for advanced miniaturized communication devices without any space and polarization constraints and also as per the demand of commercial requirement of the smaller antenna with multiple properties and low cost of fabrication.

**Acknowledgement.** The authors thank Professor (Dr.) Bhaskar Gupta and Joydeep Paul research scholar of Jadavpur University for allowing them to use the HFSS ver.13 software in his lab as well as the measurement of different parameters of fabricated antenna.

## References

1. Lin W and Wong H (2015) Wideband circular polarization reconfigurable antenna. *IEEE Transactions on Antennas Propagation* **63**, 5938–5944.
2. Lin W and Wong H (2017) Multipolarization-reconfigurable circular patch antenna with L-shaped probes. *IEEE Antennas and Wireless Propagation Letters* **16**, 1549–1552.
3. Nishamol M, Sarin V, Tony D, Aanandan C, Mohanan P and Vasudevan K (2011) An electronically reconfigurable microstrip antenna with switchable slots for polarization diversity. *IEEE Transactions on Antennas Propagation* **59**, 3424–3427.
4. Lin S, Lin Y, Li C and Lee Y (2011) Patch antenna with reconfigurable polarization. *Proceedings of Asia-Pacific Microwave Conference*, pp. 634–637.
5. Lin W and Wong H (2016) Polarization reconfigurable aperture-fed patch antenna and array. *IEEE Access* **4**, 1510–1517.
6. Kovitz J, Rajagopalan H and Rahmat-Samii Y (2015) Design and implementation of broadband MEMS RHCP/LHCP reconfigurable array using rotated E-shaped patch elements. *IEEE Transactions on Antennas Propagation* **63**, 2497–2507.
7. Peroulis D, Sarabandi K and Katehi L (2005) Design of reconfigurable slot antennas. *IEEE Transactions on Antennas Propagation* **53**, 645–654.
8. Behdad N and Sarabandi K (2006) Dual-band reconfigurable antenna with a very high tunability range. *IEEE Transactions on Antennas Propagation* **54**, 409–416.
9. Majid H, Kamal M, Rahim A, Hamid MR and Ismail MA (2012) Compact frequency-reconfigurable narrowband microstrip slot antenna. *IEEE Antennas and Wireless Propagation Letters* **11**, 616–619.
10. Hum S and Xiong HY (2010) Analysis and design of a differentially-fed frequency agile microstrip patch antenna. *IEEE Transactions on Antennas Propagation* **58**, 3122–3130.
11. Panagamuwa C, Chauraya A and Vardaxoglou Y (2008) Antenna frequency and beam reconfiguring using photoconducting switches. *Institute of Engineering Tech. Seminar on Wideband, Multiband Antennas, and Arrays for Defense or Civil Applications*, pp. 55–60.
12. Pozar D and Sanchez V (1988) Magnetic tuning of a microstrip antenna on a ferrite substrate. *Electronics Letters* **24**, 729–731.
13. Liu L and Langley R (2008) Liquid crystal tunable microstrip patch antenna. *Electronics Letters* **44**, 1179–1180.
14. Zhao Y, Huang C, Qing A and Luo X (2017) A frequency and pattern reconfigurable antenna array based on liquid crystal technology. *IEEE Photonics Journal* **9**, 1–7.
15. Bernhard J, Kiely E and Washington G (2001) A smart mechanically actuated two-layer electromagnetically coupled microstrip antenna with variable frequency, bandwidth, and antenna gain. *IEEE Transactions on Antennas Propagation* **49**, 597–601.
16. Mazlouman S, Soleimani M, Mahanfar A, Menon C and Vaughan R (2011) Pattern reconfigurable squire ring patch antenna actuated by hemispherical dielectric elastomer. *Electronics Letters* **47**, 164–165.
17. Nassar I, Weller T and Lusk C (2013) Radiating shape-shifting surface based on planar Hoberman mechanism. *IEEE Transactions on Antennas Propagation* **61**, 2861–2864.
18. Mazlouman SJ, Mahanfar A, Menon C and Vaughan R (2012) Square ring antenna with reconfigurable patch using shape memory alloy actuation. *IEEE Transactions on Antennas Propagation* **60**, 5627–5634.
19. Tawk Y, Constantine J, Avery K and Christodoulou C (2011) Implementation of a cognitive radio front-end using rotatable controlled reconfigurable antennas. *IEEE Transactions on Antennas Propagation* **59**, 1773–1778.
20. Rajya Lakshmi V and Devi P (2016) Polarization reconfigurable antenna. *International Journal of Electronics and Communication Engineering and Technology* **7**, 53–58.
21. Tawk Y, Constantine J and Christodoulou C (2010) A frequency reconfigurable rotatable microstrip antenna design. *IEEE Antennas Propagation, Society International Symposium*, pp. 1–4.
22. Sun C, Zheng H, Zhang L and Liu Y (2014) A compact frequency-reconfigurable patch antenna for Beidou (COMPASS) navigation system. *IEEE Antennas and Wireless Propagation Letters* **13**, 967–970.
23. Zhu H, Cheung S, Liu X and Yuk T (2014) Design of polarization reconfigurable antenna using metasurface. *IEEE Transactions on Antennas Propagation* **62**, 2891–2898.
24. Kushwaha N and Kumar R (2013) Design of slotted ground hexagonal microstrip patch antenna and gain improvement with FSS screen. *Progress in Electromagnetics Research B* **51**, 177–199.
25. Deshmukh AA and Ray KP (2009) Compact broadband slotted rectangular microstrip antenna. *IEEE Antennas and Wireless Propagation Letters* **8**, 1410–1413.
26. Yang G, Ali M and Dougal R (2004) A thin wideband microstrip patch antenna with two adjacent slots. *Microwave and Optical Technology Letters* **41**, 261–266.
27. Ghosal A, Das SK and Das A (2019) Multi frequency rectangular microstrip antenna with an array of L-slots. *AEU-International Journal of Electronics and Communications* **111**, 152890.
28. Kunwar A, Gautam AK and Rambabu K (2016) Design of a compact U-shaped slot triple band antenna for WLAN/WiMAX applications. *AEU-International Journal of Electronics and Communications* **71**, 309888.
29. Liu G, Gu j, Gao Z and Xu M (2019) Wideband printed slot antenna using Koch fractal metasurface structure. *International Journal of RF and Microwave Computer-Aided Engineering* **30**, e22058.
30. Kumar S, Viswakarma RK, Kumar R, Anguera J and Andujara A (2017) Slotted circularly polarized microstrip antenna for RFID application. *Radioengineering* **26**, 1025–1032.
31. Sung Y (2018) Axial ratio-tuned circularly polarized square patch antenna with long stubs. *International Journal of Antennas and Propagation* **2018**, 1–7.
32. Saraswat K, Kumar T and Harish AR (2019) A corrugated G-shaped grounded ring slot antenna for wideband circular polarization. *International Journal of Microwave and Wireless Technologies* **12**, 1–6.
33. Xu KD, Xu H, Liu y., Li J and Liu QH (2018) Microstrip patch antennas with multiple parasitic patches and shorting vias for bandwidth enhancement. *IEEE Access* **6**, 11624–11633.
34. Zhang C, Gong j, Li y and Wang Y (2018) Zeroth order mode circular microstrip antenna with patch-like radiation pattern. *IEEE Antennas and Wireless Propagation Letters* **99**, 1–8.
35. Asad Rahman M, Nishiyama E and Toyoda I (2018) A polarization reconfigurable microstrip antenna employing dual-perturbation technique. *Progress In Electromagnetics Research M* **69**, 197–206.

36. **Song T, Lee Y, Ga D and Choi J** (2012) A polarization reconfigurable microstrip patch antenna using PIN diodes. *Proceedings of APMC 2012, Kaohsiung, Taiwan*, pp. 616–618.
37. **Saravanan M and Rangachar MJS** (2018) Polarization reconfigurable square patch antenna for wireless communications. *Advanced Electromagnetics* 7, 103–108.
38. **Anantha B, Merugu I and Rao s** (2016) A novel single feed frequency and polarization reconfigurable microstrip patch antenna. *International Journal of Electronics and Communications* 16, 8–16.
39. **Hu J, Hao Z-C and Miao Z-W** (2017) Design and implementation of a planar polarization-reconfigurable antenna. *IEEE Antennas and Wireless Propagation Letters* 16, 1557–1560.
40. **Allayioti M, Kelly JR and Mitra R** (2018) Beam and polarization reconfigurable microstrip antenna based on parasitics. *Microwave and Optical Technology Letters* 60, 1460–1464.
41. **Yang X-X, Shao B-C, Yang F, Elsherbeni AZ and Gong B** (2012) A polarization reconfigurable patch antenna with loop slots on the ground plane. *IEEE Antennas and Wireless Propagation Letters* 11, 69–72.
42. **Qin P-Y, Weily AR, Guo y and Liang C-H** (2010) Polarization reconfigurable U-slot patch antenna. *IEEE Transactions on Antennas and Propagation* 58, 3383–3388.



**Murari Shaw** was born on July 4, 1980. He received his M.Tech. from Calcutta University in 2015. His research interests include Microstrip Patch antenna.



**Niranjana Mandal** was born in 1953. He received his B.Tech (Hons.) from IIT, Kharagpur, M.Tech from IIT, Delhi and Ph.D. from BITS, Rajasthan.



**Malay Gangopadhyay** was born in 1979. He received his M.Tech. from Calcutta University and Ph.D. from Jadavpur University. His research interests include Microstrip Patch antenna.